Preprint
Please cite as:
Rainone M.L., Rusi S., Torrese P. (2015): ***Mud volcanoes in central Italy: subsoil characterization through a multidisciplinary approach.*** **Geomorphology, 234, 228-242. Doi 10.1016/j.geomorph.2015.01.026**

MUD VOLCANOES IN CENTRAL ITALY: SUBSOIL CHARACTERIZATION THROUGH A MULTIDISCIPLINARY APPROACH

Rainone M.L.[a], Rusi S.[a], Torrese P.[b]

[a]Ce.R.S.GEO – Department of Engineering and Geology - "G. d'Annunzio" University of Chieti-Pescara, Italy

[b]Department of Earth and Environment Sciences, University of Pavia, Italy

Corresponding author: Rusi Sergio s.rusi@unich.it, Department of Engineering and Geology - "G. d'Annunzio" University of Chieti-Pescara, Via dei Vestini 30, Chieti, Italy, phone 0039 08713556158

Abstract

Shallow underground electrical and seismic imaging was undertaken at the Pineto (Central Italy) Mud Volcano site using 2D-3D electrical resistivity tomography (ERT) and 2D reflection seismic surveys. The hydrochemical properties of the rising fluids were assessed by means of seasonal measurements of the chemical-physical parameters, the concentrations of major ions and some natural isotopes. This mud volcano or mud lump appears as a dome of about 15x10 m in size. The height of the crater is approximately 2 m while the diameter of the crater is 2.5 m. Emission of fluids and solids (cold brine, mud, gas) occurs from this crater. Upper Pliocene-Lower Pleistocene foredeep pelitic deposits (over-compacted clays with silty-sandy levels) overlain by clayey-silty deposits crop out in the area. 2D-ERT results were used to determine the geometry of the high conductivity body related to the uprising of mud fluids and to detect changes in the deposits. Detailed reconstruction of the geometry of the shallow upward migration of mud fluids was obtained by using 3D-ERT. A shear wave reflection seismic survey was undertaken to determine stratigraphic limits and to assess the occurrence of fractured zones along which mud fluids could migrate towards the surface. The survey results seem to reveal that the uprising of deep fluids does not occur exactly below the mud volcano (MV) at present. Instead, a high conductivity body is present within a fractured zone in the pelitic deposits at approximately 60 m to the ENE. The probable occurrence of a high permeability layer

approximately between 20 m and 30 m below ground level (bgl), confined by clay deposits, gives rise to an over pressured mud fluids reservoir. Mud fluids appear to be flowing towards the surface from the reservoir up to the mud volcano crater. The interpretative conceptual model proposed by the authors is a first attempt to explain the shallow upward migration of deep mud fluids in this Central Italy MV. The results can be used to identify the uprising of fluids with similar chemical-physical properties even in areas where the superficial and morphological evidence of the volcanic bodies have been obliterated or covered.

Keywords: Mud volcano; mineralised waters; natural contamination; 2D and 3D electrical resistivity tomography; shear wave seismic reflection; Central Italy.

1. INTRODUCTION

Mud volcanism is a well-known geological phenomenon, consisting of an eruption or extrusion of mud fluids, from a highly pressurized zone to a shallower, lower-pressure zone close to the surface. These features are often associated with gas, mineralised water and fluidised sediments forming complex structures. The complex mechanisms and processes involved (Nanni and Zuppi, 1986; Kopf, 2002) are still not fully understood, in particular for some mud volcanoes (MVs). MVs are found onshore and offshore in many places on Earth and although they occur in various tectonic settings, the majority of these are located in areas subject to compressional tectonics and associated with sediment accretion at convergent margins (Aslan et al. 2001; Brown and Westbrook, 1988; Di Giulio, 1992; Higgins and Saunders, 1974; Kopf et al., 1998; Kopf, 2002; Reed et al., 1990). In Italy, mud volcanoes occur in the Western Alps and along the Apennines (Martinelli, 1999; Etiope et al. 2007) where fluid-rich, fine-grained sediments ascend within clayey deposits.

Many MVs are characterised by: an origin from thick, rapidly deposited sequences of marine clays; are generally of Tertiary age; have a structural association due to tectonic shortening and/or earthquake activity; are characterised by sediment over-pressure and accompanying fluid emission

like gas, brines, gas hydrate, salt water (Nath et al. 2008), or more rarely, oil (Etiope & Klusman, 2010) and they have polymictic assemblages of the surrounding rock present in the ejected argillaceous matrix (Ansted, 1866; Higgins and Saunders, 1974; Hovland et al. (1997); Fertl, 1976; Yassir, 1989). This article presents the methods of investigation and the results obtained from the study of the superficial portion of the MV. The study has been undertaken with a multidisciplinary approach which includes geology, hydrogeology and particularly geophysics and hydrochemistry (Figs. 1 and 2).

2D-3D electrical resistivity tomography (ERT) and 2D reflection seismic surveys were undertaken. Horizontal shear waves were used for seismic surveys (Malehmir et al., 2013); Rainone et al., 2009; Torrese et al., 2012; Signanini and Torrese, 2004). These have known benefits when compared to P waves. In fact, they achieve better imaging of complex structures in porous media and through gas. They also deliver improved resolution and pore-pressure prediction (Probert et al., 2001, Rainone and Torrese, 2007).

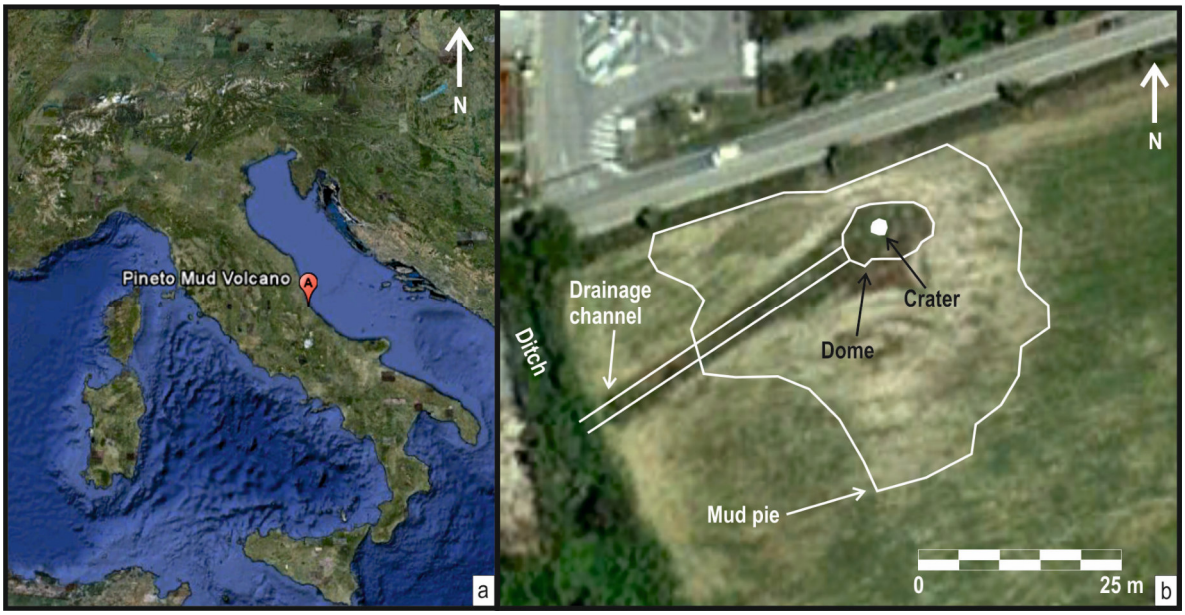

Figure 1: Geographical setting of the "Cenerone-Pineto" Mud Volcano (from Google Earth™).

Previous scientific studies on this MV only focused on the hydrochemical aspects (Desiderio and Rusi, 2004; Desiderio et al., 2007; Desiderio et al., 2010) and the environmental aspects (Colli and De Ascentis, 2003; Scalella and Di Francesco, 2004; Buccolini et al., 2003). Geochemical data

relating to MVs in Italy, including the Pineto MV, particularly in relation to gas emissions, are discussed by Etiope et al. (2003, 2007) and Etiope & Klusman (2010). The authors highlight that the gas emissions are related to N_2, CO_2 and CH_4 with percentages of 5,4 %, 0,36 % and 94,13 % respectively of the total of the gas emissions. The CH_4 flux has been estimated to be 480 mg/d m^2. The methane emissions can be connected to a microfiltration from hydrocarbons of biogenic origin according to the authors. Etiope et al. (2007) measured a helium concentration of about 16.000 ppb from the gas emissions. This value, compared with the average value of the area (146 ppb from Scalella and Di Francesco, 2004), could indicate the occurrence of deep fractures. The Pineto MV is referred to in the database for Italian MVs compiled by Martinelli and Judd (2004).

Geoelectric assessments (e.g., 3D ERT) of MVs in New Zealand are discussed in Zeyen et al. (2011), while electromagnetic applications (VLF-EM) undertaken in Taiwan have been discussed by Lin and Jeng (2010). In general, detailed shallow geophysical exploration of MVs has not been carried out (Accaino et al., 2007; Chang et al., 2010; Quo et al. (2010). The results from this study can be extended to other MVs located in similar geological contexts where the MV complex can be easily identified. The results can be particularly extended to those sites where the main body of the MVs is buried or obliterated by erosion or anthropogenic activities but where the hydrochemical properties of the fluids (gas and water) are similar and where they tend to naturally pollute the groundwater (Pilla et al., 2010).

2. MATERIAL AND METHODS

The physical-chemical parameters were determined with a multiparameter probe type WTW Multiline P4 immersed in the MV fluid. Seasonal monitoring was undertaken during the period between 2008 and 2012. Chemical analysis of major ions was undertaken during April 2009 and September 2009. Anions were determined with ionic chromatography while cations were determined with atomic adsorption. Carbonates and bi-carbonates were determined with volumetric methods. Isotope data for ^{18}O and ^{2}H were obtained using the equilibration method with CO_2 for the oxygen

isotope and the reduction to high temperature for the hydrogen isotope. The results, which are all expressed with reference to VSMOW (Vienna Standard Mean Oceanic Water) (Gonfiantini, 1978), have uncertainties of 0,1‰ and 1‰ respectively for ^{18}O and ^{2}H.

Two-dimensional resistivity tomography survey was undertaken in June 2011 along a ENE-WSW direction (Fig. 2) that is approximately perpendicular to the main axis of the buried anticlines in the area (Fig 3). The profile is 235 m in length and was obtained using 48 electrodes with a 5 m spacing. The profile intersects the MV's crater at the 12th electrode (Fig. 2). The 3D resistivity tomography was undertaken on the same day as the 2D survey. A surface snake grid comprising 12 x 4 electrodes with 10 m spacing both along the X and Y direction was used. Electrode 18, corresponding to the 12th electrode of the 2D-ERT (Fig. 2), was placed on the MV's crater.

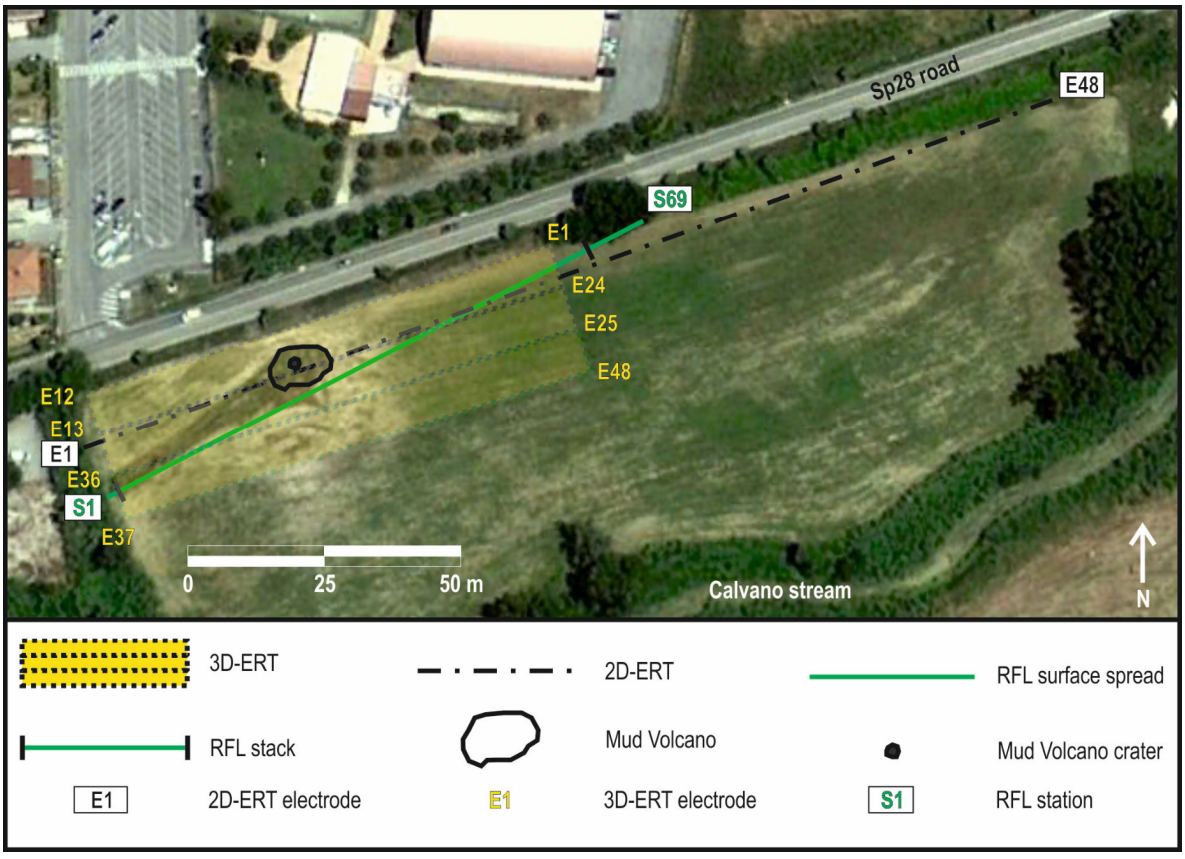

Figure 2: Geophysical survey map (from Google Earth^{TM}). Location of: 2D and 3D ERT surveys together with some electrode setting; spread and surface profile of the stack cross-section of the reflection seismic survey (RFL) together with the first and last stations setting.

The 3D survey was necessary to achieve a more detailed migration pathway of mud fluids arising at the MV's crater respect to the 2D ERT. A fully automatic multi-electrode resistivity meter SYSCAL Jr Switch-48 (max output voltage 400 V, max output current 1200 mA, max output power 100 W) by IRIS Instruments was used to collect both 2D and 3D ERT data. A sequence comprising 596 quadrupoles with a wenner-schlumberger array was used to collect 2D ERT data. A sequence comprising 270 quadrupoles was collected using all feasible X, Y and diagonal dipole-dipole array configurations to collect 3D ERT data. The injection current and supplied voltage values were determined automatically in order to receive the maximum voltage value. Spontaneous polarization was automatically compensated during the earth circuit resistance measurement. The dataset was collected with a number of stacks ranging between 3 and 6 (a standard deviation threshold of 3% was set). Good quality measurements were collected with no bad data point to reject and a standard deviation Dev=0% for 92.3% and Dev≤2% for 98.3% of 2D data and Dev=0% for 81.9% and Dev≤3% for 96.7% of 3D data. ERTLab Solver (by Multi-Phase Technologies LLC, Geostudi Astier srl) based on tetrahedral finite element modelling (FEM) was used to invert both 2D and 3D data. The earth-domain was discretized using tetrahedral elements. Different tests were carried out to find the optimal inversion parameters. The forward modeling was performed using mixed boundary conditions and a tolerance=1.0 10^{-7}. A 5% standard deviation estimate for noise was assumed to invert the dataset. The inverse modeling was performed using a maximum number of internal inverse PCG iterations of 15 and a tolerance for inverse PCG iterations of 0.001. Furthermore, the amount of roughness from one iteration to the next was controlled in order to assess layering along the X and Z directions for the 2D model and along the X, Y and Z directions for the 3D model, with the objective of identifying strong resistivity heterogeneities if present. Two dimensional and three dimensional data inversion was based on a least squares smoothness constrained approach (LaBrecque et al., 1996). Noise was appropriately managed using a data weighting algorithm (Morelli and LaBrecque, 1996) that allow to adaptively change the variance matrix after each iteration for those data points which are poorly fitted by the model. Different starting resistivity models were

tested in order to assess the correct geometry of the bodies related to the upward migration of the mud fluids. The results achieved are always congruent with the final inverse resistivity models obtained through the application of a homogeneous starting model with a background resistivity value of 5,6 ohm m for 2D ERT and 6,2 ohm m for 3D ERT. The inverse final resistivity models were chosen with a criterion based on achieving a minimum data residual obtaining congruency with the local geological setting and on taking into account the likely occurrence of artifacts of measurements in the dataset. The analysis of the chi-squared errors of the inverted models suggested that the final models were reasonably free of artifacts due to an inversion over-fit or excessive smoothing following an inversion under-fit.

A shear waves (SH) seismic reflection profile was undertaken in September 2011 along a ENE-WSW surface profile. The seismic survey was necessary to assess the occurrence of fractured zones along which mud fluids can migrate towards the surface. The survey was also undertaken to identify stratigraphic limits. Furthermore, undertaking the subsurface seismic imaging was a complementary key to assessing the shallow migration pathway of mud fluids. The profile is slightly rotated with respect to the 2D-ERT profile to avoid strong ground roughnesses related to the occurrence of the MV's dome and drainage channel. The seismic survey is 136 m in length. It crosses the MV at station 25.5, at a distance of 6 m from its crater, and cuts the 2D-ERT at station 48 (Fig. 2). An off-end spread geometry with 12 channels was used with a station and geophone strings spacing of 2 m, a source spacing of 4 m and an offset distance of 6 m, achieving a 300 % fold survey. A 24 channels Geometrics StrataView seismometer was used to collect seismic data by performing a roll along sequence with 12 active channels. A heavy metal box hammered on opposite sides with a 5 kg hammer was used for the generation of horizontal shear waves. Enhancement of the SH waves and attenuation of the compressional waves were achieved by performing the difference between the opposite shots after their polarity inversion was verified. Vertical stacking enhanced the signal-to-noise ratio by summing 8 hammer blows on average for each shot gather (4 hammer blows for each box side). An example of the quality of the dataset is shown in Fig. 7b). Each geophone string was

comprised of five 14 Hz horizontal geophones arranged along a line that is transversal to the profile. The CMP (Common-Mid-Point) processing sequence, shown in Table 1, was applied on field data in order to obtain the final two-way travel time and depth cross-sections. W-Geosoft Visual Sunt 12 Pro software interfacing with Seismic Unix modules (Cohen and Stockwell, 1999) was uses to process seismic data.

1-data import, record conversion from SEG2 to SU processing format, pre-processing editing	9- velocity analysis by constant velocity scan
2- geometry input	10- normal move out
3- surgical mute	11- stack
4- frequency filtering	12- migration
5- deconvolution	13- three traces mix
6- frequency filtering	14- automatic gain
7- elevation static	15-time to depth conversion (only for depth sections)
8- CDP sort	16-post-processing editing

TABLE 1 Processing sequence used for the reflection seismic survey.

The NMO (Normal-Move-Out) velocity model used for stacking was obtained by running a constant velocity scan on the sorted CMP gathers. The interval velocity model used for time to depth conversion was computed from the stacking velocity model using the DIX formula (Dix, 1955). Together with the FK spectrum assessment, a velocity analysis based on the dispersion of Love waves was performed on selected frequency filtered CMP gathers to verify that no surface waves affected the stack cross-sections.

3. GEOLOGICAL AND GEOMORPHOLOGICAL SETTING

Deep boreholes drilled for oil or groundwater exploration (ENI, 1972) have proven a thickness of 2000-2500 meters of foredeep pelitic deposits in the area. The compressional tectonic setting of the area is characterised by folds and blind thrusts buried under Middle Pliocene deposits (Fig. 3). Two NNW-SSE buried thrusts are the main tectonic elements of the area (Casnedi, 1983, Scisciani

and Montefalcone, 2005; Finetti et al., 2005). The nearest thrusts (the Campomare Lineament of Crescenti et al. 1980; the coastal structure of Scisciani and Montefalcone, 2005) is approximately located below the area of the MV and represents a structural high at a depth of approximately 550 m (Fig. 3).

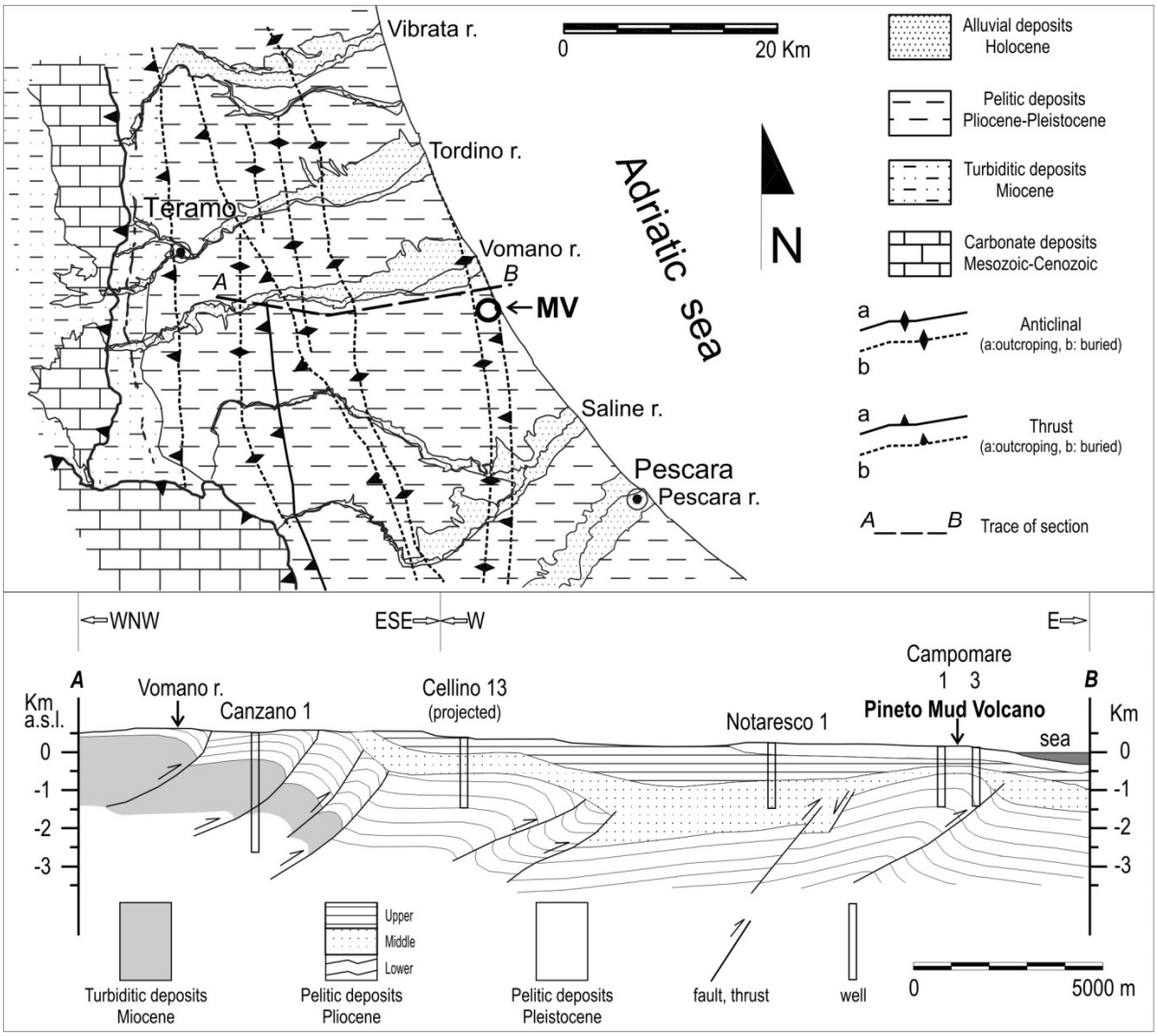

Figure 3 Geological setting of the study area. Above: structural geology schematic (modified by Crescenti et al. 1980 and Scisciani and Montefalcone 2005); Below: schematic cross-section (modified by Desiderio and Rusi 2004).

The pelitic deposits from the Upper Pliocene-Lower Pleistocene foredeep belong to the Mutignano formation (Bigi et al., 1997; Casnedi R., 1983, Casnedi et al., 1977, Crescenti et al, 1980). They consist of over-compacted clays with silty-sandy thin layers (6°-10° ENE dipping) and are overlain by clayey-silty eluvial-colluvial deposits that crop out in the area. Shallow boreholes drilled at surrounding building sites do not show the presence of alluvial deposits in spite of the closeness of

the Calvano stream and the occurrence of the bedrock pelitic deposits at a depth of approximately 10 meters. Other ditches and streams in the area run along fault systems that are oriented NW-SE and NE-SW (Bigi et al., 1997).

The MV or mud lump is located approximately 1 km to the west of the town of Pineto (Abruzzo, Central Italy, Fig. 1), on the north bank of the "Calvano" stream. The shape is that of a dome of about 15x10 m in size. The height is approximately 2 m with a crater of 2.5 m in diameter (Fig. 1b and 4). Fluids and solids (cold brine, mud, gas) are ejected from the crater (Fig. 4). Recent studies refer to only 5 MVs in the province of Teramo. The "Cenerone" MV is the only one that still has a strong eruptive activity amongst these known active MVs. Micro paleontological analyses of the clays that rise from the MV (Desiderio and Rusi 2004) date the clay-bearing sediment to the Pleistocene (Mutignano formation).

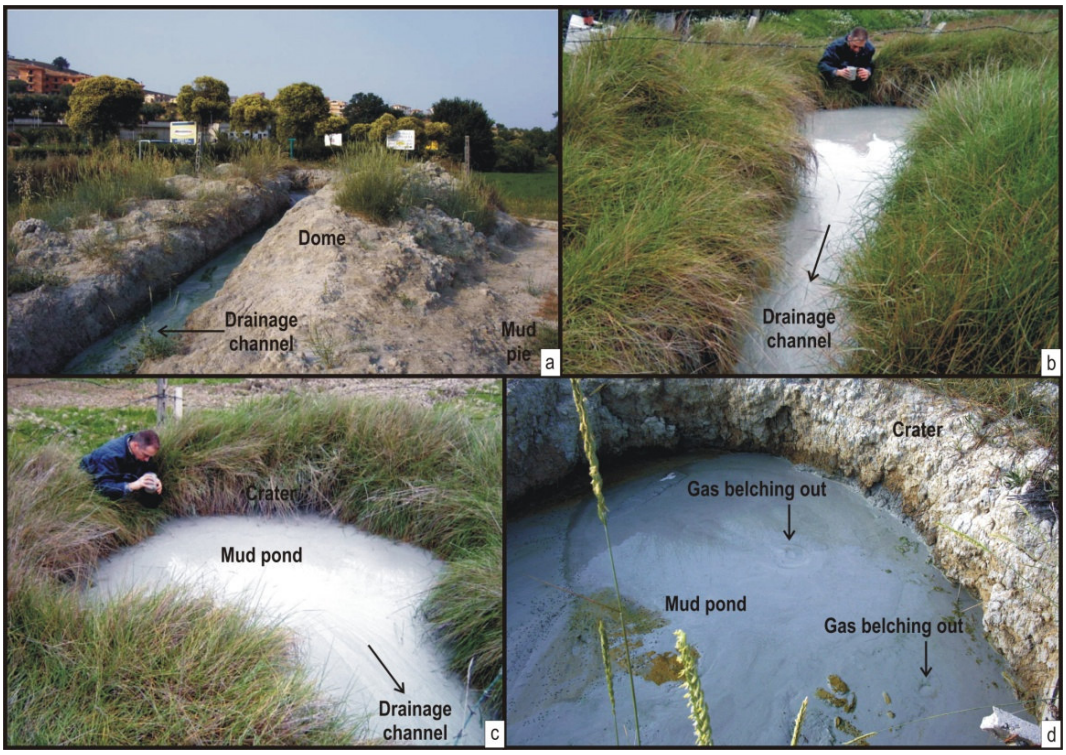

Figure 4 Images and description of the "Cenerone-Pineto" Mud Volcano.

4. HYDROGEOLOGICAL AND HYDROCHEMICAL SETTING

The local piezometric head was assessed with the data collected from 9 boreholes (Fig. 5). The piezometric surface is approximately sub-parallel to the topographical surface and is influenced by

the Calvano valley where surface water - groundwater interaction occurs. The piezometric head is approximately 2 m above the ground level in correspondence of the MV where the head is 13.6 m above sea level (asl). In fact, the main surface structure of the MV and its associated fluids are at a high elevation compared with the surrounding fields which have an elevation of approximately 11 m asl (Fig. 4).

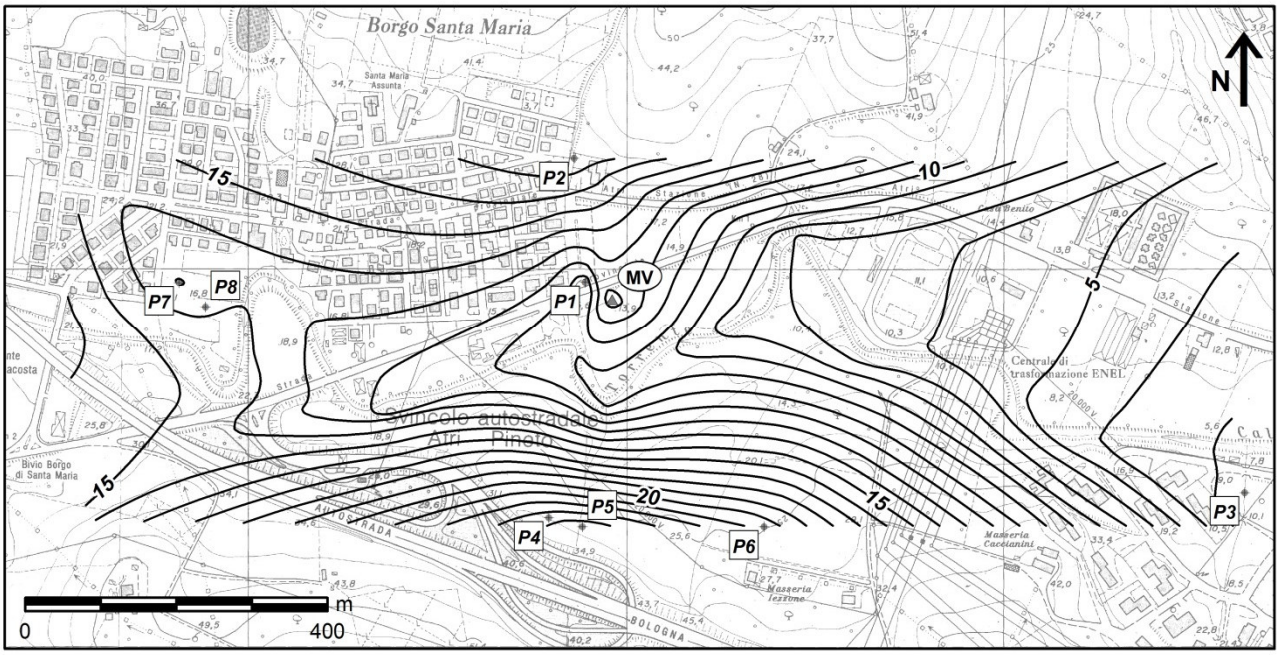

Figure 5 Piezometric surface (m asl) and location of the monitored boreholes (P1 to P8).

The waters that emerge from the MV show physico-chemical parameters with some seasonal variability (Table 2). The REDOX potential is always negative; the pH is always slightly alkaline while the electrical conductivity (EC) is constantly above 8 mS/cm.

Season	***T*** *(°C)*	***E.C.*** *(μS/cm)*	***pH***	***ORP*** *(mV)*	***Ca^{2+}*** *(mg/L)*	***Mg^{2+}*** *(mg/L)*	***Na^{+}*** *(mg/L)*	***K^{+}*** *(mg/L)*	***HCO_3^{2-}*** *(mg/L)*	***Cl^{-}*** *(mg/L)*	***SO_4^{2-}*** *(mg/L)*
Spring	15.6	8180	8.2	- 230	15.6	43.9	2612.4	41.3	831.6	3550.0	4.8
Summer	22.0	8726	8.1	- 250	27.2	52.1	3270.1	57.9	1022.8	4749.2	7.3

TABLE 2 Chemical-physical parameters and the major ion concentration of the MV's pond water. T: Temperature; EC: electrical conductivity (25 °C); pH: negative logarithm of the activity of the hydronium ion; ORP: redox potential.

The results of the groundwater physico-chemical parameters obtained from logs of the monitoring boreholes surrounding the MV (fig. 5) show completely different values (Table 3) when compared to the values from the MV. The EC and REDOX potential vary between 1,26 and 2,20 mS/cm and between +89 and +149 mV respectively.

The chemistry of the groundwater (Table 2 and fig. 6) is sodium chloride with ionic formula Na, K, Mg - Cl, HCO_3, SO_4 and with a low content of sulphates.

Well	***T*** *(°C)*	***pH***	***E. C.*** *(mS/cm)*	***ORP*** *(mV)*
P1	17,4	7,7 – 8,2	1,76 – 1,77	+113 – +120
P2	15 – 15,3	7,3 – 7,7	1,55 – 1,68	+147 – +148
P3	11,9 – 12	8,0 – 8,4	1,26	+89 – +92
P4	15,5 – 16,8	8,2 – 8,5	0,94 – 2,29	+96 – +112
P6	16,0 – 16,4	7,4 – 7,9	1,73 – 2,20	+129 – +149
P7	14,7	8,1 – 8,2	1,48	+98 – +100
P8	16,8 – 16,9	7,7 – 8,0	1,59 – 1,60	+112 – +113
MV	**13 – 22**	**8,1**	**8,12**	**- 220**

TABLE 3 Chemical-Physical parameters of the groundwater from surrounding observation boreholes (locations are shown in fig. 5). The observation borehole values are the min and max of the log within each observation borehole while the MV values represent the average values within the measurement periods.

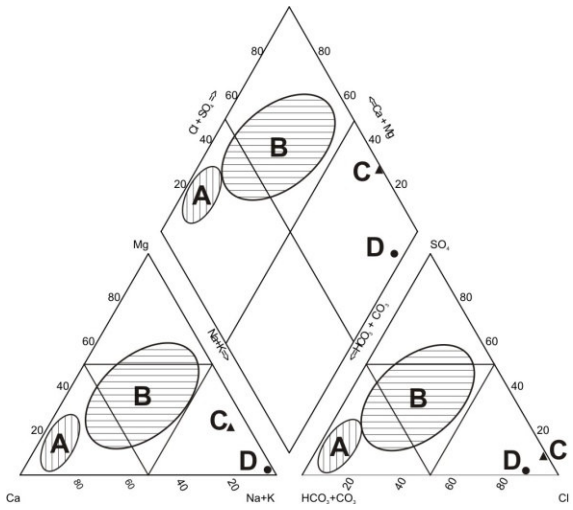

Figure 6 Piper diagram which compares the MV water to the groundwater of other hydrogeological contexts of Central Italy: A) carbonate aquifers; B) alluvial aquifers; C) sea water; D) MV.

The isotopic data for ^{18}O e ^{2}H from the MV (Table 4) is less negative than that of the groundwater encountered in the alluvial deposits within the valley and the carbonate structures of the Apennines. The average estimated elevation of recharge calculated from isotopic concentrations using both the mathematical relationships of Barbieri et al. (2002) and that of Conversini and Tazioli (1993) is not plausible. The waters from the MV are by no means connected to recent recharge waters given that $\delta^{18}O$ and $\delta^{2}H$ values from the MV's groundwater are more positive than the surrounding waters.

Group	***Altitude*** *(m asl)*	$\delta^{18}O$	$\delta^{2}H$
Carbonate aquifer springs (1)	310	-9,13	-60,16
	670	-8,13	-51,90
	825	-9,87	-66,15
	1150	-10,01	-67,43
	1210	-10,08	-68,01
Alluvial deposit boreholes (2)	104	-9,45	-61,29
	450	-7,98	-50,27
	570	-8,48	-54,30
	600	-8,14	-55,59
MV	**15**	**-6,47**	**-42,26**

TABLE 4 $\delta^{18}O$ and $\delta^{2}H$ average values within the groundwater in the areas surrounding the Site. (1) The springs are located in carbonate deposits described in the geological setting shown in Fig.3, from Desiderio et al. (2005). (2) The boreholes are located in alluvial deposits described in the geological setting shown in Fig. 3, from Desiderio and Rusi (2004).

In accordance with the "mud dome" type A model (Kopf, 2002), the data collected indicates, from a hydrochemical point of view, the existence of a fluid that is constituted of saline water, gas (mostly CH_4) and mud that rises to the surface through a clayey lithological sequence. The fluid rises in isolation from the surrounding hydrogeological context.

Groundwater with similar chemistry is often encountered in the alluvial deposits and foredeep deposits of the Apennines (Desiderio et al. 2001, 2010; Desiderio and Rusi, 2004; Nanni and Vivalda 1999). Desiderio and Rusi (2004) and Palmucci and Rusi (2014) have identified mineralised groundwater with a Na/Cl ratio close to that of sea water, a sodium-chloride hydrochemical facies with low sulphates and positive values of $\delta^{18}O$ and $\delta^{2}H$.

These groundwaters often emerge at surface in correspondence of structural highs and thrusts or in correspondence of tectonic lineaments that crop out or are buried. When these tectonic structures come into contact with basal saline waters, they vehicle the saline waters to the surface with the aid of N_2, CO_2 and CH_4 gases. When the uprising of the saline waters intercepts groundwater in alluvial aquifers, the chemical-physical parameters are attenuated. If the shallow groundwater flow in the alluvial deposits is particularly high, the original chemical-physical properties of the saline waters can be totally obliterated. In these cases, multidisciplinary geophysical studies are particularly important as they assist with the identification of the pathways that the uprising fluids follow.

5. GEOPHYSICAL INVESTIGATIONS

5.1. 2D electrical resistivity tomography

The low resistivity area appearing just below the MV in the apparent resistivity pseudo-section (Fig. 7a) appears to be an artefact of measurements produced by the occurrence of very low resistivity values at the ground surface (MV's crater); this area is affected by a low penetration. Furthermore, the sub-vertical high resistivity area located at approximately 30 m to the ENE of the MV, which is observed in the apparent resistivity pseudo-section, does not appear to be connected to the occurrence of any real subsurface body as shown on the inverse resistivity section.

The final inverse resistivity section that fits the true data with a root mean square (RMS) error of 4.86 % at the 12^{th} iteration (Fig. 8) is showed in Fig. 9a. It reveals the occurrence of a low resistivity body (body B) located 50 m to the ENE of the MV at a depth between 17 m and 33 m. This body is

characterised by low resistivity values ranging between 3.4 and 3.9 ohm m. The inverse resistivity section doesn't show any low resistivity body occurring just below the MV.

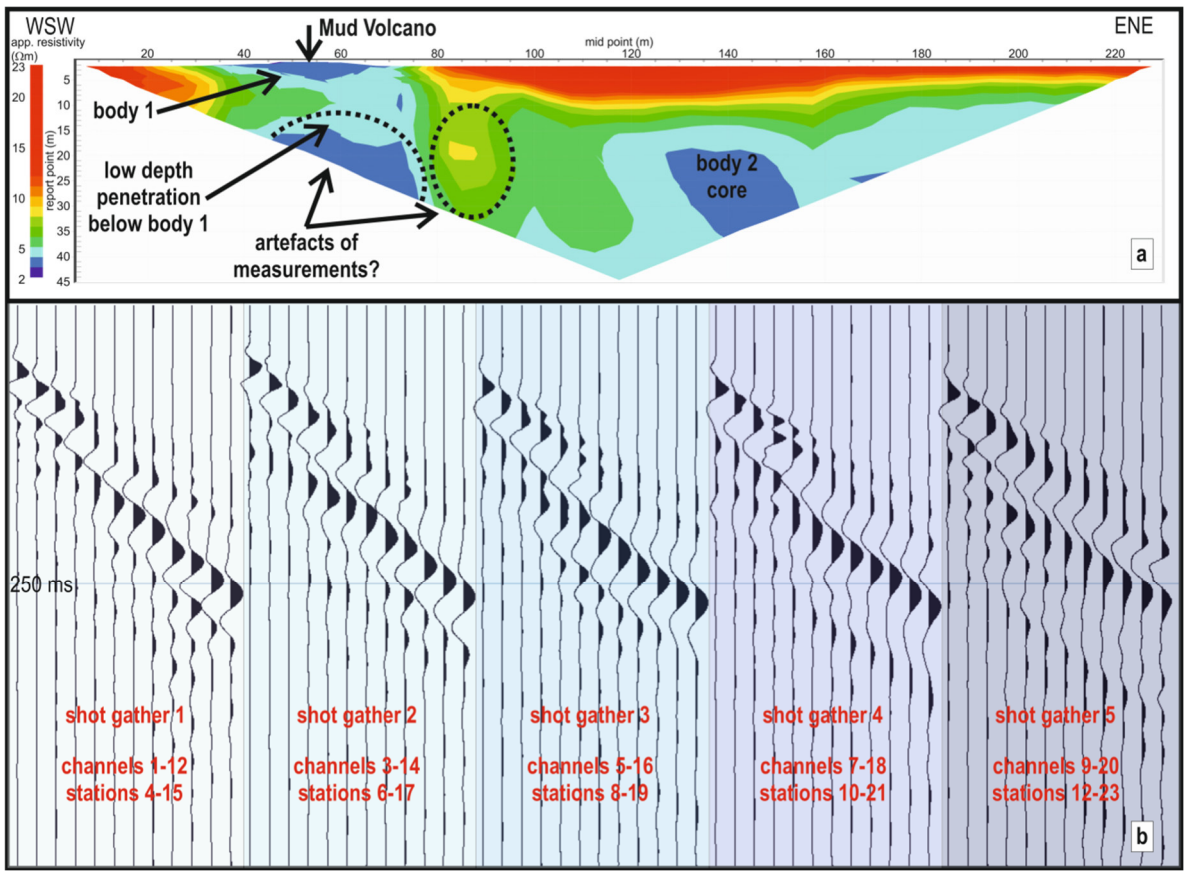

Figure 7 (a) Apparent resistivity pseudo-section of the 2D-ERT: body 1 represents the shallow MV's root, body 2 suggests the occurrence of a low resistivity anomaly at depth, the low resistivity area appearing just below the MV (where low penetration occurs) and the high resistivity area occurring between bodies 1 and 2 appear to be artefacts of the measurements (see main text). (b) First five shot gathers of the SH waves reflection survey showing the quality of the raw dataset (first 500 ms showed): an off-end spread geometry was used with each shot gather comprised of 12 traces.

The fact that body B in the inverse resistivity section of Fig. 9a shows lower resistivity values than the surrounding clay deposits, suggests that high salinity mud fluids occur. Body A in Fig. 9a, which has resistivity values ranging between 1.88-5.51 ohm m, represents the shallow MV's root that shows the lowest resistivity values (between 1.88-3.47 ohm m) near the surface where fluids with high salinity stagnate in deposits of a clayey-silty matrix. Figs. 9c and 12c show the low resistivity bodies A and B: the likely connection between them is shown by 2D ERT. The two surface bodies C

and D, respectively to the ENE and WSW of body A (Fig. 9a), show resistivity values higher than 9 ohm m.

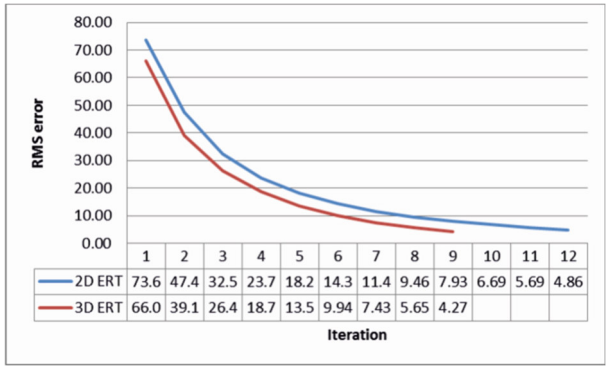

	1	2	3	4	5	6	7	8	9	10	11	12
2D ERT	73.6	47.4	32.5	23.7	18.2	14.3	11.4	9.46	7.93	6.69	5.69	4.86
3D ERT	66.0	39.1	26.4	18.7	13.5	9.94	7.43	5.65	4.27			

Figure 8 Variation of RMS error with respect to the iteration number for the final inverted resistivity models. Convergence was reached after 12 and 9 iterations for 2D ERT and 3D ERT respectively (see main text).

These results are consistent with the occurrence of clayey-silty drift deposits that are about 10 m thick (thinning toward ENE), overlying saturated over-compacted clay deposits, as confirmed from logs of surrounding shallow boreholes (Fig. 5). Available evidence suggests that clay deposits contain a high permeability layer that is saturated with mud fluids (body B). The piezometric head is 13,6 m asl in correspondence of the MV, whereas the main fresh groundwater level should be about 11 m asl (Fig. 5) as boreholes surrounding the MV revealed. The likely high permeability layer that is saturated with mud fluids (body B) seems to be a localised aquifer with mineralised water isolated with respect to the adjacent groundwater system.

A locally more complete and accurate survey was required to verify the connection between bodies A and B (also for slightly different Y values with respect to the 2D ERT plane section). The survey would also allow verification of the migration of mud fluids from depth towards the MV's crater. Therefore, a 3D ERT survey was undertaken.

5.2. 3D electrical resistivity tomography

Fig. 9b is a perspective view extracted from the final inverse resistivity model that fits the true data with an RMS error of 4.27 % at the 9th iteration (Fig. 8): a range of resistivity values between 1.58-4.2 ohm m is observed. This plume corresponds to body A, the western part of the body B and the pathway that seems to connect them, due to the migration of mud fluids. The occurrence of this plume of mud fluids and the connection between bodies A and B are shown with a different perspective in Figures 10b, 10c, 10e.

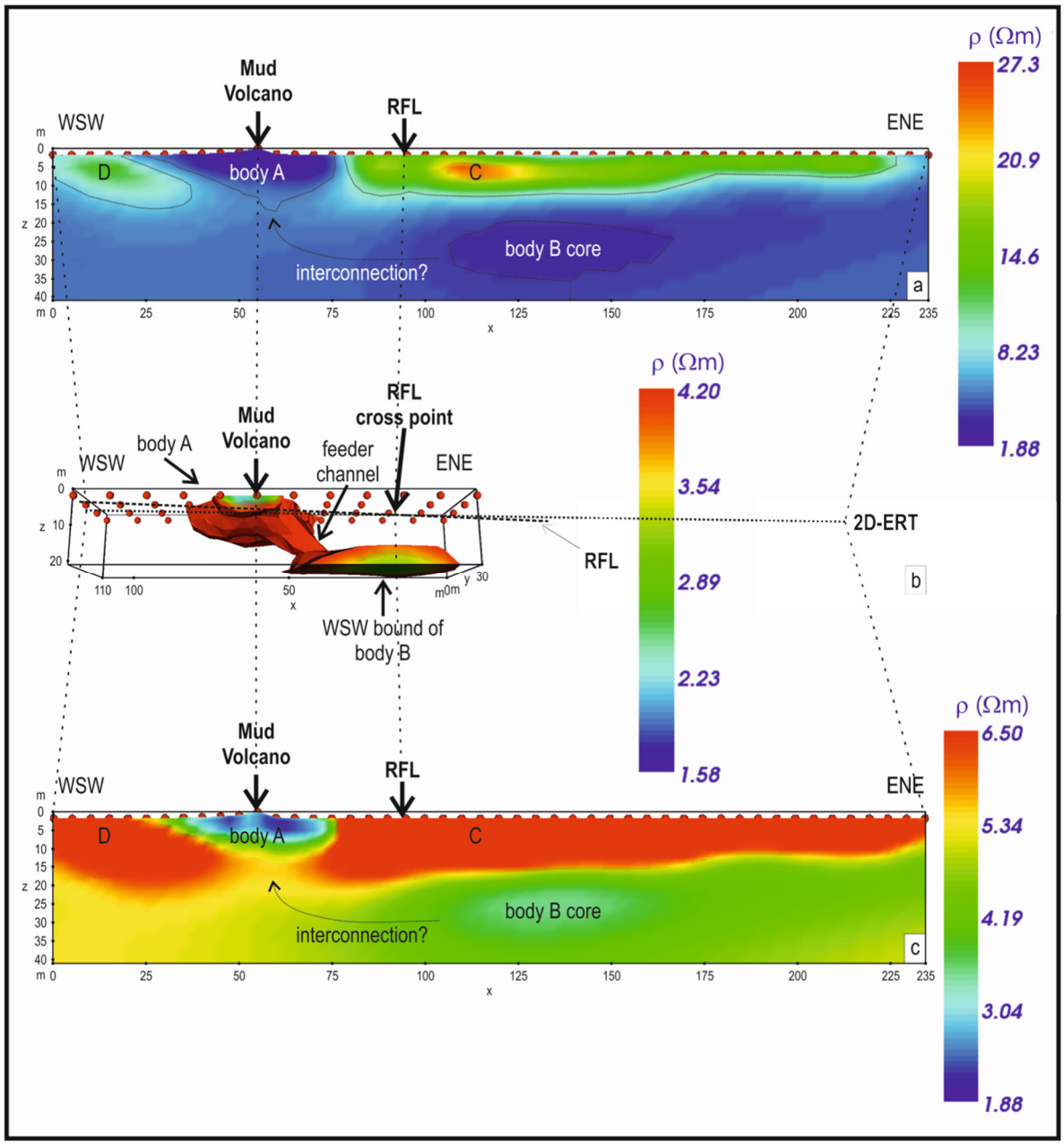

Figure 9 (a) 2D-ERT inverse resistivity section with a full scale range: body A represents the shallow MV's root, body B that shows lower resistivity values compared to the surrounding clay deposits, which suggests that high salinity mud fluids occur (in a high permeability layer?). (b) Lowest resistivity range plume extraction from 3D-ERT inverse resistivity model showing the likely occurrence and shallow migration of mud fluids: body A, the WSW bound of body B and a feeder channel between them are shown. (c) 2D-ERT inverse resistivity section with narrow scale range of values enhancing the low resistivity variation related to the occurrence of mud fluids. The connection between bodies A and B is not clear in the 2D ERT; however, the 3D ERT shows a feeder channel suggesting a very localized (fractures?) near vertical migration of mud fluids towards the MV's crater (see main text).

Figure 10d shows the X-Z plane slice corresponding to the plane surface of the 2D-ERT. Plume resistivity values appear fairly different from the surrounding media (Fig. 10a). The near vertical migration of mud fluids (the likely connection between bodies A and B) appears very localised as it occur along a fracture. A shear wave reflection seismic survey was undertaken to assess the occurrence of fractures along which mud fluids could migrate towards the surface and determine stratigraphic limits.

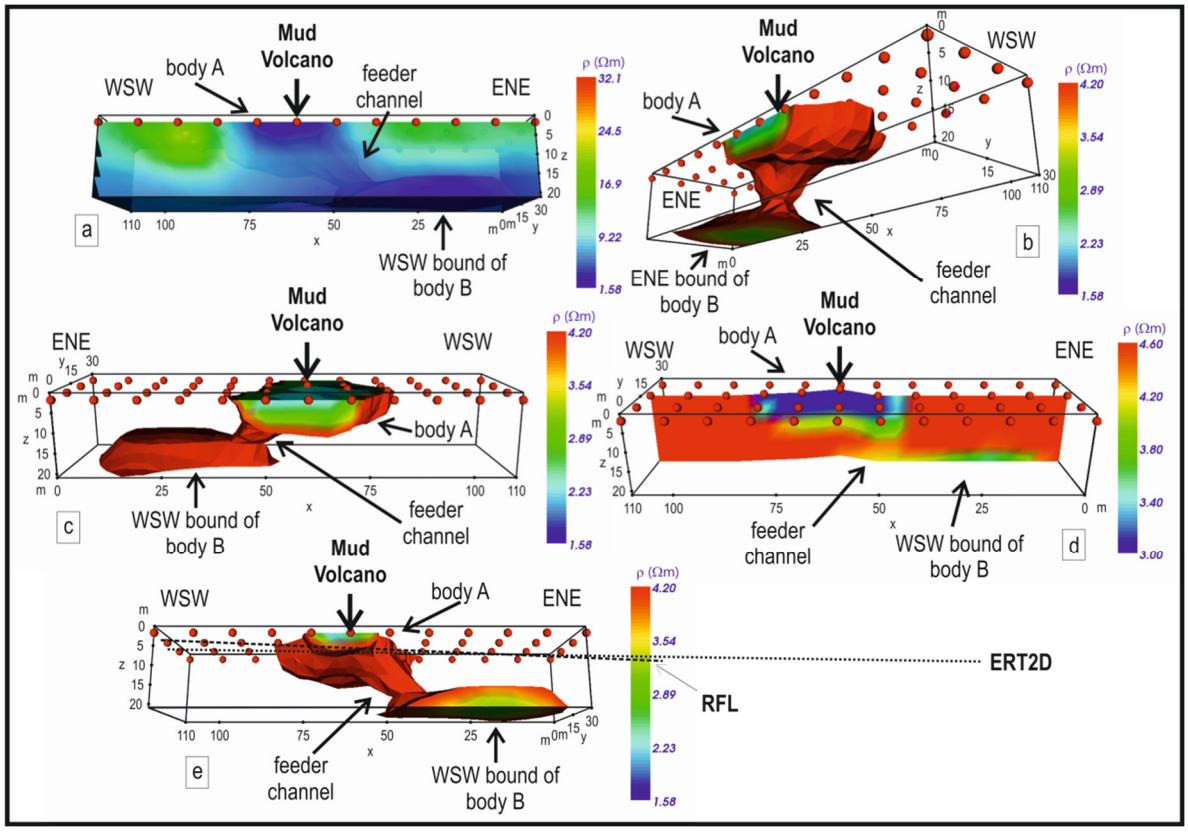

Figure 10 3D-ERT inverse resistivity model: (a) full scale range transparent model with 4.2 ohm m iso-surface showing occurrence of mud fluids; (b, c, e) different perspective views of the 1.58-4.2 ohm m range plume extraction showing body A (the shallow MV's root), the WSW bound of body B (the shallow mud fluids reservoir?) and a feeder channel suggesting the migration of mud fluids between bodies B and A, towards the MV's crater; (d) xz slice at y=10 m (this 2D visualization can be directly compared with 2D ERT sections shown in Figs. 9a, 9c and 12c) with a narrow scale range of values showing the likely connection between bodies B and A (mud fluids migration).

5.3. Reflection seismic survey

Fig. 11a shows the two-way travel time migrated cross-section with a frequency content ranging between 35 and 110 Hz. The shallow MV root is affected by upward bending of layers between 90 and 180 ms (8-15 m) and by a main central fracture at station 25.5 (location of the MV's crater) as indicating the uprising of fluids.

The seismic cross-section is affected by several fractures that interrupt the continuity of reflectors as shown in Fig.11b. The NMO velocity model reveals the occurrence of low velocity zones, probably related to highly fractured regions within the over-compacted clay deposits (heavily fractured areas in Fig. 11b).

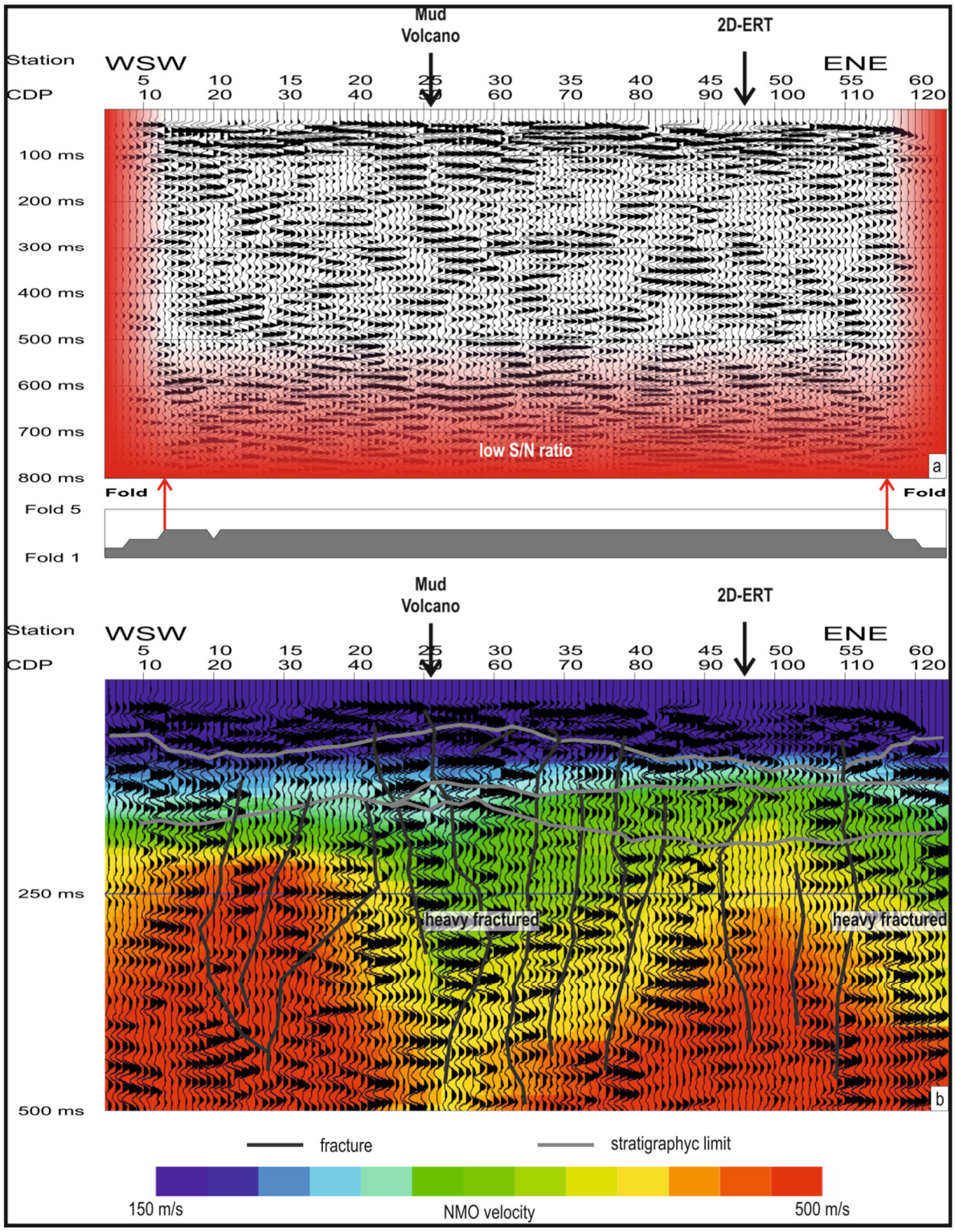

Figure 11 SH waves reflection survey: (a) two-way travel time migrate cross-section: the use of a 300 % fold shows a fair signal-to-noise ratio in the section, but S/N ratio decreases for two-way travel times larger than 500 ms and at the lateral borders of the section where fold strongly decreases; (b) NMO velocity model (obtained by running a constant velocity scan on the sorted CMP gathers) and a line drawing overlaying the two-way travel time migrate section: for times greater than 200 ms the occurrence of low velocity zones appears to be related to highly fractured regions within the over-compacted clay deposits (heavily fractured).

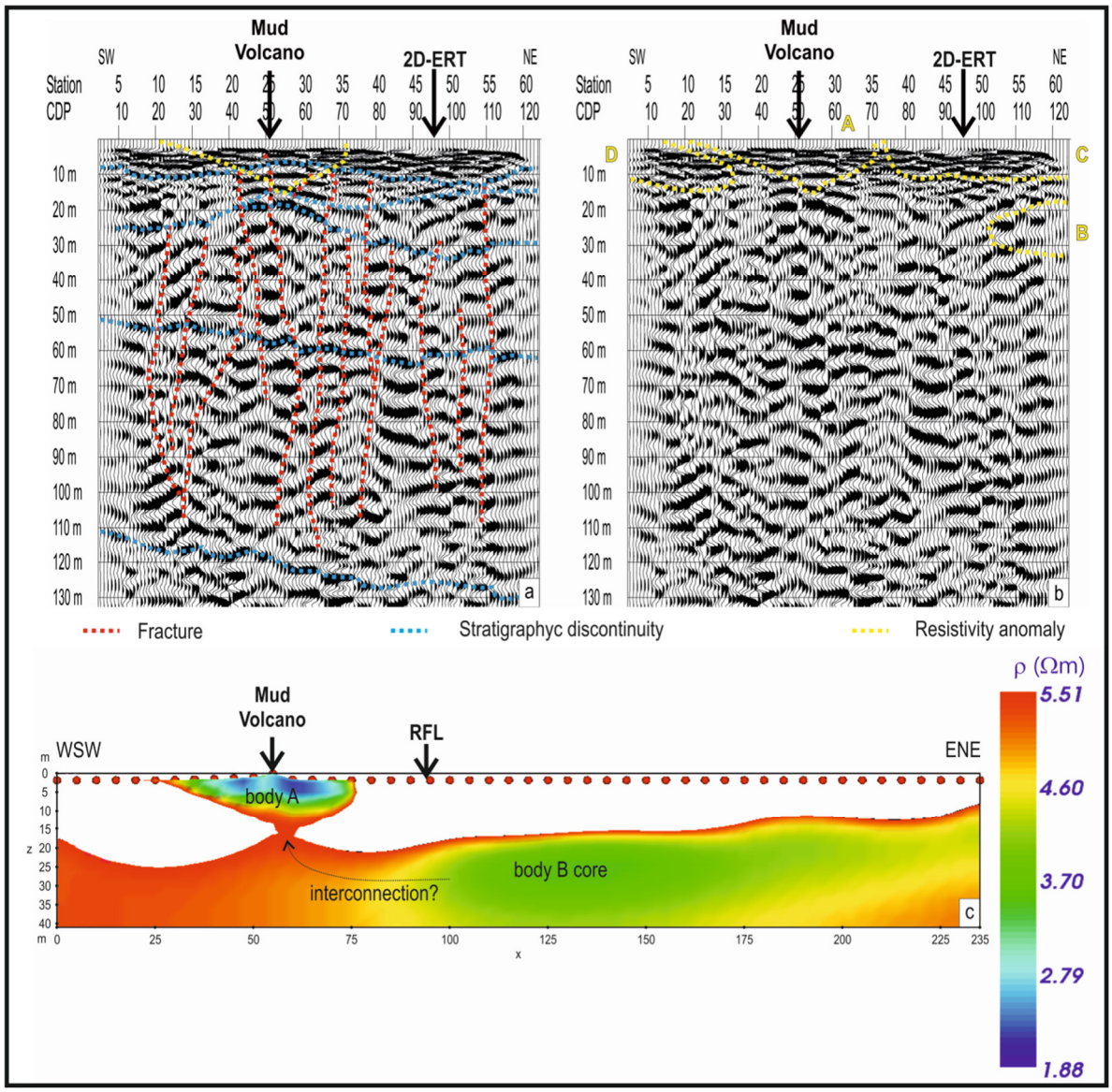

Figure 12 (a) Line drawing interpretation of the depth seismic cross-section identifying the stratigraphic limits (light blue lines), the fractures (red lines) and the MV's root (yellow line, body A shown in Fig. 12c): note the fair congruence between the seismic and the resistivity imaging (bodies A and B in Fig, 12c). (b) Depth seismic cross-section marked by the resistivity anomalies shown in Fig. 9a). (c) Low resistivity range extraction from the 2D-ERT inverse resistivity section showing the geometry of body A (marked on the depth cross-section of Figs. 12a and 12b) and the likely point of connection between bodies B and A (as identified by the 3D ERT, see the main text). Note that the worm-like patterns shown at large depth on the depth seismic cross-section (and not shown by the related time cross-section in Figs. 11a and 11b) are not due to a ringing effect, but are due to the shortening of the X axis so that the assessment could be undertaken using the same X and Z scale).

Fig. 12a shows the interpreted depth cross-section on which five stratigraphic limits are drawn. The two deeper limits are related to stratigraphic limits occurring within the over-compacted clay

deposits (Mutignano formation) that are affected by a slight basal unconformity. The shallower three limits are related to the stratigraphic limit between the clayey-silty drift deposits with a variable thickness of approximately 10 m and the over-compacted clay deposits which may have an interbedded layer that has a relatively high permeability when compared to the surrounding deposits. This is consistent with the resistivity anomalies identified from results of the 2D-ERT survey (Figs. 12b, 12c) and confirmed by the logs of surrounding shallow boreholes (Fig. 5 and Table 3). The high permeability layer appears to be affected by six deep fractures, four of which are cutting the layer for its entire thickness. The deep fractures affect only the over-compacted clay deposits. The only deep fracture that appears to affect the clayey-silty drift deposits is the fracture located at station 25.5 (location of the MV's crater, Fig. 12a). The faulting of the drift deposits cannot be related to recent tectonic activity. It is more likely connected to hydrostatic pressure that is induced by the uprising of fluids along deep fractures that affect the over-compacted clay deposits and that is related to tectonic activity.

6. INTEGRATING THE GEOELECTRICAL DATA WITH THE HYDROCHEMICAL DATA

An initial attempt to estimate the clay content and the hydraulic parameters (Table 5) of the mud fluids reservoir (the high permeability layer) and the surrounding clay deposits was undertaken using Archie's law (Archie, 1942) (1):

$$F = \frac{a}{\varphi^m} = \frac{\rho}{\rho_w} \qquad (1)$$

with F = formation factor, a = tortuosity factor, φ = porosity, m = cementation factor, ρ = resistivity of the rock filled with only water, ρ_w = water resistivity.

	Resistivity, ρ (ohm m)	**Salinity** (NaCl, g/l)	**Formation factor, F**
MV's pond water	1.21 (June)	7.09 (average)	
Fresh groundwater	6.02	0.2	
Mud fluids reservoir	3.6		2.98
Clay deposits	5.3		0.88

TABLE 5 Resistivity and salinity values for MV's pond water and fresh groundwater, formation factor for the mud fluids reservoir and the surrounding clay deposits.

The total porosity of a formation can be estimated from the formation resistivity and the aquifer groundwater resistivity using Archie's law. This approach was considered feasible under the assumption that no mixing of saline and fresh waters was occurring which is supported by the hydrochemical assessment undertaken from the monitoring boreholes surrounding the MV (Table 3).

Using Archie's law, the resulting formation factor obtained for the mud fluids reservoir is 2.98 (using an average resistivity value ρ=3.6 ohm m for the mud fluids reservoir and ρ_ω=1.21 ohm m for the water which is the average resistivity value of the MV's pond water , Table 5). This indicates that the total porosity is 43 % if a=1 and m= 1.3 are used in (1) which in turn indicates a probable presence of clay content (discarding the effects of fracturing). In fact, the resulting formation factor is close to the limit of 2.5 which would correspond to a clay content of the formation of 47.6 % (spherical particles with cube arrangement, Astier, 1971). This is the maximum clay content that deposits with low clay content can have. A formation factor of 0.88 (less than the maximum limit of 2.5) is obtained if Archie's law is applied to the surrounding clay deposits (using the values showed in Table 5 for the average resistivity of the clay deposits and the sampled fresh groundwater). This formation factor yields a porosity of 110 % which is not possible (Astier, 1971). As these formations definitely do have some clay content, the limits of applicability of Archie's law are evident (Waxman and Smits, 1968; Worthington, 1985). However, it does allow inferring that the surrounding clay deposits are actually constituted of clays and that the mud fluids reservoir has a much lower clay content.

Given the presence of groundwater at different salinity conditions, the authors used the algorithm proposed by Ryjov and Sudoplatov (1990). This algorithm can be used to estimate the clay

content in clayey-sandy formations knowing the resistivity of the formation and the salinity of the groundwater (Shevnin *et al.,* 2006; Shevnin *et al.*, 2007). Fracturing of the formation is neglected. An indicative estimate (Fig. 13, Table 6) of the clay content (valid for CEC of clay = 1.73 g/l; clay porosity = 0.55; sand porosity = 0.22; radius of clay pores = $3*10^{-9}$ m) for the mud fluids reservoir was obtained and estimated to be approximately 5 % (with total porosity of 23 %) while the clay content of the surrounding clay deposits was estimated to be 33 % (with 16 % total porosity).

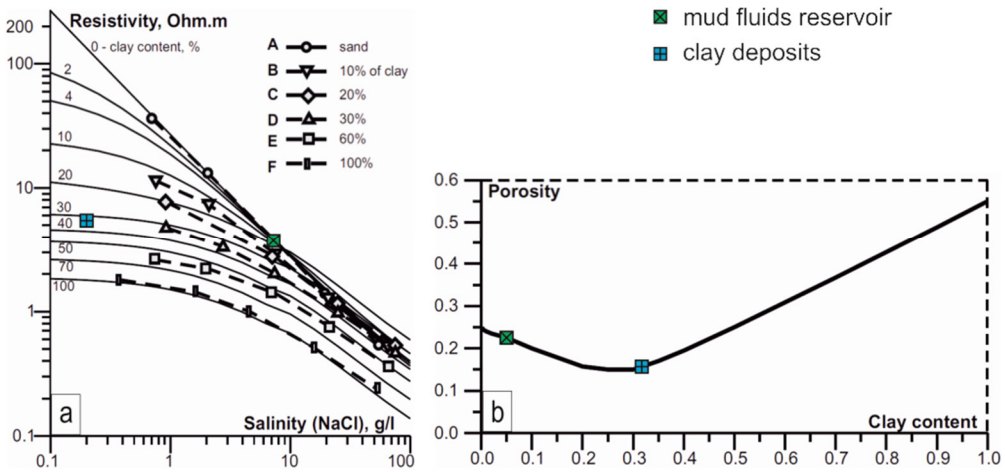

Figure 13 (a) Theoretical graphs of soil resistivity versus groundwater salinity for different clay content (for clayey-sandy soils showing the clay content determined for the mud fluids reservoir and the clay deposits, the graph is valid for CEC of clay=1.73 g/l, clay porosity=0.55, sand porosity=0.22, radius of clay pores=$3*10^{-9}$ m). The values presented in Table 5 were used for the average resistivity of the mud fluids reservoir, the clay deposits and the salinity of the sampled MV's pond water and fresh groundwater (see main text). (b) Relationship between soil porosity of the clayey-sandy soil and its clay content showing the porosity value determined for the mud fluids reservoir and the clay deposits on the basis of their clay content evaluated by means of the graph showed in (a), Modified after Shevnin et al. (2006).

The values shown in Table 5 for the average resistivity of the mud fluids reservoir, the clay deposits, the salinity of the MV's pond water (empirically determined from the average resistivity value of the MV's pond water in June) and the sampled fresh groundwater were used for this assessment. Although these results do not represent an accurate estimate of the clay content of the formation, they do explain the different permeabilities of the two formations and the consequent

diffusion of the mud fluids. These fluids remain confined under pressure within the formation with the highest permeability and eventually make their way to the surface through the crater of the MV.

	Clay content (%) (Ryjov and Sudoplatov,1990)	**Total Porosity, ϕ (%)** (Ryjov and Sudoplatov,1990)	**Hydraulic conductivity (m/d)** (Shevnin et al., 2006)
Mud fluids reservoir	5	23	0,1
Clay deposits	33	16	0,003

TABLE 6 Clay content, total porosity and hydraulic conductivity estimates for the mud fluids reservoir and the clay deposits.

7. CONCLUSIONS

The occurrence of a low resistivity body (3.4-3.9 ohm m), approximately between 17 m and 33 m below ground level, was revealed by 2D electrical resistivity tomography. The low resistivity body is not located directly below the mud volcano but appears to be located at approximately 60 m to the ENE. The fact that this body shows lower resistivity values than the surrounding over-compacted clay deposits suggests that it's congruent with the occurrence of a high permeability layer that is saturated with high salinity mud fluids. 3D electrical resistivity tomography appears to confirm the connection between the mud fluids reservoir and the MV's crater. Based on these results, it is reasonable to assume that mud fluids would flow sub-horizontally along the high permeability layer at depth and would then flow upward towards the MV's crater. The sub-vertical migration of mud fluids appears to be very localised as it occurs along a fracture. The shear wave reflection seismic survey indicates that the shallow root of the MV is affected by upward bending of layers between 8 and 15 m of depth. A main central fracture coinciding with the MV's crater, thus allowing the uprising of mud fluids, is also shown by the shear wave reflection seismic. On the basis of the obtained geophysical and hydrochemical results, the authors suggest a reasonable interpretative conceptual model. Mud fluids are likely to rise along deep fractures within the over-compacted clay deposits

located on the ENE portion of the seismic cross-section where the shear wave velocity model indicates the occurrence of a fractured zone (Fig. 14a).

The mud fluids could then flow into a high permeability layer that would act as an over pressured mud fluids reservoir (Fig. 14b). This is consistent with the fact that mud fluids flow out of the MV's crater that is approximately 2 m above ground level.

This localised aquifer with mineralised groundwater appears to be disconnected from the main groundwater system as revealed by boreholes surrounding the MV.

Although there are four fractures that completely cut through the mud fluids reservoir and extend to the stratigraphic limit of the overlying drift deposits, mud fluids can reach the surface only at the MV's crater due to the localised thinning of the drift deposits in correspondence of the MV (Fig. 12c, 14).

Hydrostatic pressure would induce failure of the drift deposits and upward bending of the layers. It cannot be excluded that in the past, mud fluids rose along the deep fracture located just below the MV (Fig. 14a). This is consistent with the shear waves low velocity zone revealed by the velocity analysis (Fig. 11b). It's also possible that there were more emissions of mud fluids at surface before agricultural activities and other anthropogenic activities obliterated these features at the site. Fig. 14b shows the occurrence of a low resistivity body at a distance of 135 m to the ENE of the MV which could probably be connected to a MV remnant. Here too, mud fluids could reach the surface from the same over pressurised mud fluids reservoir because thinning of the drift deposits also occurs here similarly to what is observed for the main MV.

An initial estimate of some of the hydrogeological properties of the mud fluids reservoir and the surrounding over-compacted clay deposits was obtained from the integrated analysis of the hydrochemical and resistivity data collected for this study.

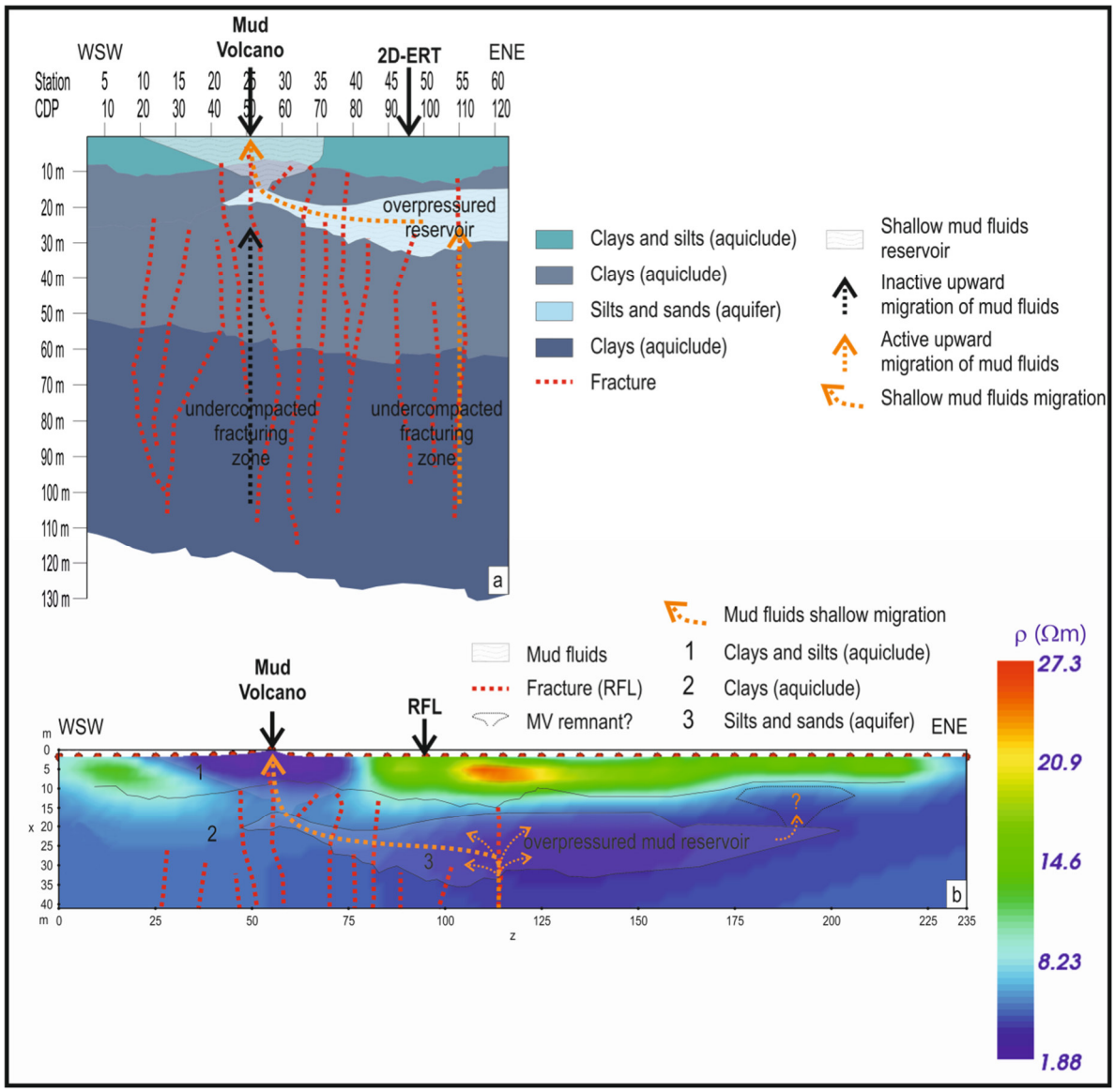

Figure 14 Proposed conceptual model showing the migration pathway of the mud fluids from a deep fractured zone within the over-compacted clay deposits to the MV's crater; interpretative model overlying (a) the depth seismic cross-section and (b) the 2D-ERT section (only fractures revealed by the seismic reflection survey are shown). Mud fluids could rise along deep fractures within the over-compacted clay deposits (active upward migration of mud fluids); mud fluids could flow into a high permeability layer (shallow mud fluids reservoir) that would act as an over pressured mud fluids reservoir; mud fluids could still reach the surface only at the MV's crater due to the localised thinning of the drift deposits in correspondence of the MV where hydrostatic pressure would induce failure and upward bending of the layers.

The interpretative conceptual model proposed by the authors is a first attempt to explain the shallow upward migration of deep mud fluids (with highly mineralised waters) in this MV in Central Italy. The integrated use of 2D-3D electrical resistivity tomography and shear waves reflection

seismic surveys permitted the reconstruction of the local hydrogeological system where the uprising of highly mineralised mud fluids is clearly revealed by the presence of the MV. It should be noted that this approach can also be extended to the investigation of naturally polluted groundwater where the upward migration of deep fluids does not show evidence at the surface because of obliteration from erosion or anthropogenic activities. Therefore, the results from this study can be extended to other MVs located in similar geological contexts.

Acknowledgements

The authors wish to thank prof. Patrizio Signanini for the precious advice, Sara Di Benedetto, Fabio Colantonio and Antonio Gennarini for the precious collaboration and the professional geologists which provided boreholes and penetrometric tests data.

REFERENCES

Accaino F., Bratus A., Conti S., Fontana D., Tinivella U. 2007. Fluid seepage in mud volcanoes of the northern Apennines: an integrated geophysical and geological study. Journal of Applied Geophysics 63 (2), 90–101. doi: 10.1016/j.jappgeo.2007.06.002.

Ansted D. T. 1866. On the mud volcanoes of the Crimea, and on the relation of these and similar phenomena to deposits of petroleum. Proc. R. Inst. G. B., IV, 628–640.

Archie G.E. 1942. The electrical resistivity log as an aid in determining some reservoir characteristics. Journal of Petroleum Technology 1, 55−62.

Aslan, A., Warne, A.G., White, W.A., Guevara, E.H., Smyth, R.C., Raney, J.A., Gibeaut, J.C. 2001. Mud volcanoes of the Orinoco Delta, Eastern Venezuela. Geomorphology 41 (4), 323–336. doi: 10.1016/S0169-555X(01)00065-4

Astier J.L. 1971. Géophysique appliquée à l'hydrogéologie. Masson & C^{ie} Editeurs, 277 p.

Barbieri M., D'Amelio L., Desiderio G., Marchetti A., Nanni T., Petitta M., Rusi S., Tallini M. 2002. Gli isotopi ambientali (^{18}O, ^{2}H e $^{87}Sr/^{86}Sr$) nelle acque sorgive dell'Appennino abruzzese:

considerazioni sui circuiti sotterranei negli acquiferi carbonatici. Proceedings of 1st Congress AIGA, Chieti, Italy, 69-81.

Bigi S., Centamore E., Nisio S. 1997. Elementi di tettonica quaternaria nell'area pedeappenninica marchigiano-abruzzese. Italian Journal of Quaternary Sciences. 10 (2), 359-362.

Brown K.M. and Westbrook G.K. 1988. Mud diapirism and subcretion in the Barbados Ridge Complex. Tectonics 7, 613– 640.

Buccolini M., Crescenti U., Rusi S., Sciarra N. 2003. Itinerario n. 6 della Guida Geologica Regionale Abruzzo. Società Geologica Italiana, BE-MA editrice, Roma.

Casnedi R. 1983. Hydrocarbon-bearing Submarine Fan System of Cellino Formation, Central Italy. American Association Petroleum Geologist Bulletin, 67 (3), 359-370.

Casnedi R., Follador U., Moruzzi G. 1977. Geologia del campo gassifero di Cellino (Abruzzo), Bollettino della Società Geologica Italiana 95, 891-901.

Conversini P., Tazioli G.S. 1993. Indagini idrogeologiche nella media e alta valle del fiume Menotre, Umbria orientale. Atti Ticinensi di Scienze della Terra 36, 153-164.

Crescenti U., D'amato C., Balduzzi A., Tonna M. 1980. Il Plio-Pleistocene del sottosuolo abruzzese-marchigiano tra Ascoli Piceno e Pescara. Geologica Romana 19, 63-84.

Chang P., Yang T., Chyi L.L., Hong W. 2010. Electrical Resistivity Variations Before and After the Pingtung Earthquake in the Wushanting Mud Volcano Area in Southwestern Taiwan. Journal of Environmental and Engineering Geophysics 15 (4), 219–231. doi: 10.2113/JEEG15.4.219.

Cohen J. K., Stockwell Jr. J. W. 1999. Seismic Unix Release 33: a free package for seismic research and processing. Center for Wave Phenomena, Colorado School of Mines, Sercel, SN 368 Filed Equipment Technical manual, December 1987.

Colli B., De Ascentiis A. 2003. Il Cenerone – Vulcanello di fango di Pineto. De Rerum Natura 35/36, 10-15.

Desiderio G., Nanni T., Rusi S., Vivalda P. 2001. The mineralised springs of the Marche and Abruzzi foredeep (central Italy): some remarks on the hydrochemical and tectonics features. 10th

international simposium on Water Rock interaction. Villasimius (CA), 2001, R. Cidu Ed. A.A. Balkema Publishers, 493-496.

Desiderio G., Rusi S. 2004. Hydrogeology and hydrochemistry of the mineralised waters of the Abruzzo and Molise foredeep (Central Italy). Bollettino della Società Geologica Italiana, 123 (3), 373-389.

Desiderio G., Ferracuti L., Rusi S., Tatangelo F. 2005. Il contributo degli isotopi naturali ^{18}O e ^{2}H nello studio delle idrostrutture carbonatiche abruzzesi e delle acque mineralizzate nell'area abruzzese e molisana. Giornale di Geologia Applicata 2, 453–458. doi: 10.1474/GGA.2005–02.0–66.0092.

Desiderio G., Ferracuti L., Rusi S. 2007. Structural-Stratigraphic Setting of Middle Adriatic Alluvial Plains and its Control on Quantitative and Qualitative Groundwater Circulation, Memorie Descrittive della Carta Geologica d'Italia 76, 147-162.

Desiderio G., Rusi S., Tatangelo F. 2010. Hydrogeochemical characterization of Abruzzo groundwaters and relative anomalies. Italian Journal of Geosciences, 129 (2), 207-222. doi: 10.3301/IJG.2010.05.

Di Giulio A. 1992. The evolution of the Western Ligurian Flysch Units and the role of mud diapirism in ancient accretionary prisms (Maritime Alps, NW Italy). Geologische Rundschau 81 (3), 655–668. doi:10.1007/BF01791383.

Dix C.H. 1955. Seismic velocities from surface measurements. Geophysics 20, 68-86.

ENI. 1972. Acque dolci sotterranee. Inventario dei dati raccolti dall'Agip durante la ricerca di idrocarburi in Italia. Grafica Palombi Roma.

Etiope G., Martinelli G., Caracausi A., Italiano F. 2007. Methane seeps and mud volcanoes in Italy: Gas origin, fractionation and emission to the atmosphere. Geophysical Research Letters 34, L14303. doi:10.1029/2007gl030341.

Etiope G., Caracausi A., Favara R., Italiano F., Baciu C. 2003. Reply to comment by A. Kopf on "Methane emission from the mud volcanoes of Sicily (Italy)", and notice on CH_4 flux data from

European mud volcanoes. Geophysical Research Letters 30 (2), 1094, 66-1/66-4. doi: 10.1029/2002GL016287.

Etiope G., Klusman R.W. 2010. Microseepage in drylands: Flux and implications in the global atmospheric source/sink budget of methane. Global and Planetary Change 72, 265–274. doi:10.1016/j.gloplacha.2010.01.002.

Fertl W. H. 1976. Abnormal Formation Pressures: Implications to Exploration Drilling and Production of Oil and Gas. Development in Petroleum Science, vol. II, 382 pp., Elsevier Sci., New York, 1976.

Finetti I.R., Calamita F., Crescenti U., Del Ben A., Forlin E., Pipan M., Prizzon A., Rusciadelli G., Scisciani V. 2005. Crustal geological cross-section across Central Italy from the Corsica Basin to the Adriatic sea based on geological and CROP seismic data. In: CROP PROJECT: deep seismic exploration of the central Mediterranean and Italy, edited by Finetti I.R. Elsevier.

Gonfiantini R. 1978. Standards for stable isotope measurements in natural compounds. Nature 271, 534-536.

Higgins G.E., Saunders J.B. 1974. Mud volcanoes: their nature and origin: Contribution to geology and paleobiology of the caribbean and adjacent areas. Verhandlungen Naturforschenden Gesellschaft Basel 84, 101–152.

Hovland, M., Hill, A., Stokes D. 1997. The structure and geomorphology of the Dashgil mud volcano, Azerbaijan. Geomorphology 21 (1), 1-15 doi: 10.1016/S0169-555X(97)00034-2

Kopf A., Robertson A.H.F., Clennell M.B., Flecker R. 1998. Mechanism of mud extrusion on the Mediterranean Ridge. Geo-Marine Letters 18 (2), 97–114. doi: 10.1007/s003670050058.

Kopf A.J. 2002. Significance of mud volcanism. Reviews of Geophysics 40 (2), 1005, doi:10.1029/2000RG000093.

LaBrecque D.J., Miletto M., Daily W., Ramirez A., Owen E. 1996. The effects of noise on Occam's Inversion of resistivity tomography data. Geophysics 61, 538–548. doi: 10.1190/1.1443980

Lin M.J., Jeng Y. 2010. Application of the VLF-EM method with EEMD to the study of a mud volcano in southern Taiwan. Geomorphology 119, 97–110. doi: 10.1016/j.geomorph.2010.02.021.

Malehmir A., Saleem M.U., Bastani M. 2013. High-resolution reflection seismic investigations of quick-clay and associated formations at a landslide scar in southwest Sweden. Journal of Applied Geophysics, 92, 84-102. doi: 10.1016/j.jappgeo.2013.02.013

Martinelli G. 1999. Mud volcanoes of Italy: a review. Giornale di Geologia, serie 3, 61, 107-113.

Martinelli G., Judd A. 2004. Mud volcanoes of Italy. Geological Journal, 39, 49–61. doi: 10.1002/gj.943.

Morelli G., LaBrecque D.J. 1996. Advances in ERT inverse modelling. European Journal of Environmental and Engineering Geophysical Society 1 (2), 171–186.

Nanni T., Vivalda P. 1999. Le acque salate dell'avanfossa marchigiana: origine, chimismo e caratteri strutturali delle zone di emergenza. Bollettino della Società Geologica Italiana 118, 191-215.

Nanni T., Zuppi G.M. 1986. Acque salate e circolazione profonda in relazione all'assetto strutturale del fronte adriatico e padano dell'Appennino. Memorie della Società Geologica Italiana 35, 979-986.

Nath B., Jiin-Shuh J., Ming-Kuo L., Huai-Jen Y., Chia-Chuan L. 2008. Geochemistry of high arsenic groundwater in Chia-Nan plain, Southwestern Taiwan: possible sources and reactive transport of arsenic. Journal of Contaminant Hydrology, 99, 85–96. doi: 10.1016/j.jconhyd.2008.04.005.

Palmucci W., Rusi S. 2014. Boron-rich groundwater in Central Eastern Italy: a hydrogeochemical and statistical approach to define origin and distribution. Environ. Earth Sci. doi 10.1007/s12665-014-3384-5

Pilla G., Torrese P., Bersan M. 2010. Application of hydrochemical and preliminary geophysical surveys within the study of the saltwater uprising occurring in the Oltrepò Pavese plain aquifer. Bollettino di Geofisica Teorica e Applicata 51 (4), 301-323.

Probert T., Bryan R., Ronen S., Engelmark F., Akenteiva E., Browning G., Rowson C., Bakhshiev F., Kawai N., Nazarov A. 2001. Mud Volcanoes And Shear-wave Imaging - an Example 4C Test Line In the Caspian Sea. Proceeding of Society of Exploration Geophysicists Annual Meeting, September 9 - 14, San Antonio, Texas.

Quo, C. S., Hung, C. C., Hsing C. L., Yen, C. C. 2010. Mud volcanoes along the Chishan fault in Southwestern Taiwan: A release bend model. Geomorphology 118 (1-2), 188–198. doi:10.1016/j.geomorph.2009.12.018

Rainone M.L., Torrese P. 2007. HR reflection surveys for seismic imaging of unstable slopes. Proceeding of SAGEEP 20th Annual Meeting, 528-536, Denver, CO-USA, 1-5 April 2007.

Rainone M. L., Torrese P., Signanini P., Foresta M., Giles J. 2009. Smart and effective SH waves acquisition in shallow seismic reflection surveys. Proceeding of SAGEEP 22nd Annual Meeting, 768-774, Fort Worth, TX-USA, 29 March-2 April 2009.

Reed D.L., Silver E.R., Tagudin J.E., Shipley T.H., Vrolijk P. 1990. Relations between mud volcanoes, thrust deformation, slope sedimentation, and gas hydrate, offshore north Panama. Marine and Petroleum Geology 7, 44–54.

Ryjov A.A., Sudoplatov A.D. 1990. The calculation of specific electrical conductivity for sandy – clayed rocks and the usage of functional cross–plots for the decision of hydrogeological problems. In the book: "Scientific and technical achievements and advanced experience in the field of geology and mineral deposits research. Moscow, 27–41. (In Russian).

Scalella G., Di Francesco R. 2004. Le sorgenti connesse ai vulcanelli di fango nel territorio teramano: valorizzazione, conservazione e tutela. Geologia dell'Ambiente 3, 90-96.

Scisciani V., Montefalcone R. 2005. Neogene-Quaternary evolution of the Central Apennine thrust front: constraints from sequence and forward balancing of a regional cross-section. Bollettino della Società Geologica Italiana 124/3, 579-599.

Shevnin V., Delgado-Rodríguez O., Mousatov A., Ryjov A. 2006. Estimation of hydraulic conductivity on clay content in soil determined from resistivity data. Geofísica Internacional 45 (3), 195-207.

Shevnin V., Mousatov A., Ryjov A., Delgado-Rodriquez O. 2007. Estimation of clay content in soil based on resistivity modeling and laboratory measurements. Geophysical Prospecting, 55, 265–275. doi: 10.1111/j.1365-2478.2007.00599.x

Signanini P., Torrese P. 2004. Application of high resolution shear wave seismic methods to a geotechnical problem. Bulletin of Engineering Geology and the Environment, 63 (4), 329-336.

Torrese P., Rainone M.L., Rusi S., Signanini P. 2012. Shallow electrical and seismic imaging of the Pineto Mud Volcano (Central Italy). Proceeding of SAGEEP 25th Annual Meeting, 545-557, Tucson AZ-USA, 25-29 March 2012.

Waxman M.H., Smits L.J.M. 1968. Electrical conductivities in oil-bearing shaly sand. Society of Petroleum Engineers Journal 8, 107−122.

Worthington P.E. 1985. The evolution of shaly-sand concepts in reservoir evaluation. The Log Analyst, January−February, 23−40.

Yassir, N. A. 1989. Mud volcanoes and the behaviour of overpressured clays and silts. PhD thesis, 249 pp., University of London, UK.

Zeyen H., Pessel M., Ledésert B., Hébert R., Bartier D., Sabin M., Lallemant S. 2011. 3D electrical resistivity imaging of the near-surface structure of mud-volcano vents. Tectonophysics, 509, 181–190. doi:10.1016/j.tecto.2011.05.007.